Radiative and nonradiative charge transfer in $He^+ + H$ collisions at low energy

B. Zygelman and A. Dalgarno
Harvard-Smithsonian Center for Astrophysics, 60 Garden Street, Cambridge, Massachusetts 02138

M. Kimura
Argonne National Laboratory, Argonne, Illinois 60439
and Department of Physics, Rice University, Houston, Texas 77251

N. F. Lane
Department of Physics and Rice Quantum Institute, Rice University, Houston, Texas 77251
(Received 17 November 1988)

We report the calculated cross sections for the removal of He^+ ions in collisions with hydrogen atoms for the collision energy range between 0.01 meV and 100 eV. Radiative association is the dominant mechanism at the low-energy extreme and for collision energies above 10 meV radiative charge transfer is dominant. Above 8 eV the radiative processes are negligible, and direct charge transfer is the primary removal mechanism. Using a quantum-mechanical method, we obtain the spectrum of the emitted radiation for the radiative charge transfer process at several collision energies. The emission spectrum has a main peak at wavelengths near 113 nm, which corresponds to the energy difference between the $A\,^1\Sigma^+$ and $X\,^1\Sigma^+$ states of the molecular ion HeH^+ at large internuclear distances. At higher collision energies, significant contributions to the emission spectra occur at shorter wavelengths, and distinct peaks appear. We interpret these peaks as a result of orbiting in the outgoing channel.

I. INTRODUCTION

Collisions of He^+ ions and neutral hydrogen atoms are important in a wide range of astrophysical environments.[1] The He^+ ions may be removed by nonradiative charge transfer

$$He^+ + H \rightarrow He + H^+ , \tag{1}$$

by radiative charge transfer,

$$He^+ + H \rightarrow He + H^+ + h\nu , \tag{2}$$

and by radiative association,

$$He^+ + H \rightarrow HeH^+ + h\nu . \tag{3}$$

Estimates of the rate coefficients for the radiative processes (2) and (3) have been presented by Sando, Cohen, and Dalgarno[2] for temperatures in the range $1 < T < 1000$ K. At collision energies above a few eV the nonradiative process (1) becomes more rapid.

The radiative processes are driven by the interaction of the collision system with the radiation field. Several procedures have been used to calculate the cross sections for radiative collisions and the relationships between them have been demonstrated.[3] The direct charge transfer process arises through transitions between different molecular states driven by the perturbation caused by the nuclear motion.[4,5] It may be investigated with a molecular-orbital expansion method, provided the electron translation factor is taken into account.[6] Because the collision energy considered is low, it sufficed to include only molecular states which correspond to the initial $A\,^1\Sigma^+$ and final $X\,^1\Sigma^+$ channels.

In this paper, we report calculations of the cross sections for direct and radiative processes which occur in the collisions of He^+ with H at energies up to 100 eV and we present the rate coefficient of the processes (2) and (3) for temperatures up to 1000 K.

II. THEORY

A. Nonradiative charge transfer

Full configuration-interaction calculations were performed to obtain the Born-Oppenheimer eigenvalues and eigenfunctions of the electronic Hamiltonian of the molecule HeH^+. A linear combination of Slater determinants with Slater-type orbitals was employed. The calculated asymptotic values for the electronic energies are 2.5000 and 2.9031 hartrees for the $A\,^1\Sigma^+$ and $X\,^1\Sigma^+$ states, respectively; these compare favorably with the exact nonrelativistic values 2.5000 and 2.9037 hartrees, respectively.

In the quantum-mechanical formalism, the scattering wave function is expanded in terms of the Born-Oppenheimer wave functions $\phi_i(\mathbf{r},\mathbf{R})$ modified by the electron translation factor (ETF).[6,7] If $\chi_i^a(\mathbf{R})$ is the wave function of the nuclear motion in the electronic state i, we write (unless otherwise stated, atomic units are used throughout)

$$\Psi(\mathbf{r},\mathbf{R}) = \sum_i \exp\left[\left[\frac{1}{\mu}\mathbf{S}\cdot\nabla_R\right]\right]\phi_i(\mathbf{r},\mathbf{R})\chi_i^a(\mathbf{R}) , \tag{4}$$

where μ is the reduced mass,

$$\mathbf{S} = \tfrac{1}{2} f_i(\mathbf{r},\mathbf{R})\mathbf{r} , \tag{5}$$

and the f_i's are switching functions that incorporate the

molecular character of the ETF. After some manipulation, the coupled equations for $\chi_i^a(\mathbf{R})$ may be obtained in the matrix form

$$\left[\frac{-1}{2\mu}[\underline{I}\nabla_R - i(\underline{\mathbf{P}}+\underline{\mathbf{A}})]^2+\underline{V}\right]\underline{\chi}^a(\mathbf{R})=E\underline{\chi}^a(\mathbf{R}) , \tag{6}$$

where

$$\mathbf{P}_{ij}=\langle\phi_i|-i\nabla_R|\phi_j\rangle , \tag{7a}$$

$$\mathbf{A}_{ij}=i(E_i-E_j)\langle\phi_i|\mathbf{S}|\phi_j\rangle , \tag{7b}$$

$$V_{ij}(R)=\delta_{ij}V_i(R) , \tag{7c}$$

E is the energy of the nuclear motion in the center-of-mass frame, and $\underline{I}$ is the identity matrix. In Eq. (7), $\mathbf{P}_{ij}$ represents the nonadiabatic coupling, $\mathbf{A}_{ij}$ its ETF correction, and $V_i(R)$ is the potential energy for the ith Born-Oppenheimer state. The set of coupled equations (6) can be put in a form more convenient for numerical solution by transforming to a diabatic representation. The transformation from adiabatic to diabatic representation is achieved by introducing a new set of nuclear wave functions $\underline{\chi}^d(R)$ defined by

$$\underline{\chi}^a(R)=\underline{C}(R)\underline{\chi}^d(R) ,$$

where

$$\frac{d\underline{C}}{dR}+\underline{P}_R\underline{C}=0$$

and

$$\underline{P}_R\equiv\underline{\mathbf{P}}\cdot\hat{\mathbf{R}} . \tag{8}$$

Then, the coupled equations can be rewritten in the diabatic representation as

$$\left[\frac{-1}{2\mu}\nabla_R^2\underline{I}+\underline{U}(R)+E\underline{I}\right]\underline{\chi}^d(\mathbf{R})=0 , \tag{9}$$

where

$$\underline{U}(R)=\underline{C}^{-1}(R)\underline{V}(R)\underline{C}(R) . \tag{10}$$

The coupled equations (9) may be solved numerically using the log-derivative algorithm[8] to determine the scattering matrix and the cross sections for nonradiative charge transfer.

B. Radiative charge transfer and radiative association

The radiative charge transfer cross sections may be calculated using the formula[3]

$$\sigma=\int_0^{\omega_{\max}}d\omega\frac{d\sigma}{d\omega} , \tag{11}$$

where

$$\frac{d\sigma}{d\omega}=\frac{8}{3}\left[\frac{\pi\mu}{k_a}\right]^2\frac{1}{c^3}\omega^3\sum_J[JM_{J,J-1}^2(k_a,k_b)+(J+1)M_{J,J+1}^2(k_a,k_b)]$$

and

$$M_{J,J'}(k_a,k_b)\equiv\frac{1}{\sqrt{k_ak_b}}\int_0^\infty dR s_J(k_aR)D(R)f_{J'}(k_bR) , \tag{12}$$

k_a and k_b being the wave numbers of the initial and final motion. The partial waves $f_J(kR)$ and $s_J(kR)$ are regular solutions of the homogeneous radial equations

$$\left[\frac{d^2}{dR^2}-\frac{J(J+1)}{R^2}-2\mu[V_a(R)-V_a(\infty)]+k^2\right]s_J(kR)=0 , \tag{13}$$

$$\left[\frac{d^2}{dR^2}-\frac{J(J+1)}{R^2}-2\mu[V_b(R)-V_b(\infty)]+k^2\right]f_J(kR)=0 ,$$

where $V_b(R)$ and $V_a(R)$ are the potential-energy curves for the initial excited, and final ground states, respectively. The wave numbers are given by

$$k_b\equiv\{2\mu[E-\hbar\omega-V_b(\infty)]\}^{1/2} ,$$

$$k_a\equiv\{2\mu[E-V_a(\infty)]\}^{1/2} ,$$

where ω is the angular frequency of the emitted photon, E is the total collision energy in the incident channel in the center-of-mass frame, and $D(R)$ is the transition dipole moment connecting the two electronic states. The wave functions obey the asymptotic boundary conditions

$$f_J(kR)\rightarrow\left[\frac{2}{\pi}\right]^{1/2}\sin\left[kR-\frac{J\pi}{2}+\delta_J(a)\right] ,$$

$$s_J(kR)\rightarrow\left[\frac{2}{\pi}\right]^{1/2}\sin\left[kR-\frac{J\pi}{2}+\delta_J(b)\right] ,$$

where $\delta_J(a)$ and $\delta_J(b)$ are the phase shifts for the channels a and b, respectively.

We have also calculated the total cross section for the collision-induced radiative removal of He^+ by hydrogen atoms, which is the sum of the cross sections for radiative charge transfer and radiative association processes. To calculate this total cross section, we use the optical potential method.[3,9,10] In this essentially semiclassical approximation, the probability per unit time for a radiative transition from the excited $A\,^1\Sigma^+$ state to the ground $X\,^1\Sigma^+$ state to occur is represented by the imaginary part of a complex potential (the optical potential). The amplitude $F_a(R)$ for the system to be in the excited $A\,^1\Sigma^+$ state, at internuclear distance R, is a solution of the equation

$$\left[\frac{-1}{2\mu}\nabla_R^2+V_a(R)-E\right]F_a(\mathbf{R})=\frac{i}{2}A(R)F_a(\mathbf{R}) , \tag{14}$$

$$A(R)=\tfrac{4}{3}D^2(R)\frac{|V_b(R)-V_a(R)|^3}{c^3} .$$

Equation (14) is solved by using a partial-wave decomposition of the amplitude $F_a(\mathbf{R})$. Because the right-hand side of (14) is imaginary, the partial-wave solutions have complex phase shifts, the imaginary parts of which reflect the loss of flux from each incoming channel. The total cross section for radiative decay is given by[9]

$$\sigma = \frac{\pi}{k_a^2} \sum_J^{\infty} (2J+1)[1-\exp(-4\eta_J)] , \tag{15}$$

where η_J is the imaginary part of the complex phase shift for the Jth partial wave. Because the right-hand side of (14) is proportional to $1/c^3$ and, therefore, is very small, it is appropriate to use the distorted-wave approximation to the phase shift[3]

$$\eta_J = \frac{\pi\mu}{2k_a} \int_0^{\infty} dR\, |s_J(k_a R)|^2 A(R) . \tag{16}$$

The difference between the total radiative-decay cross section and the radiative charge transfer cross section is the cross section for radiative association.

III. RESULTS AND DISCUSSIONS

A. Radiative charge transfer and association

Shown in Fig. 1 are the adiabatic potential curves for the initial $A\,^1\Sigma^+$ and final $X\,^1\Sigma^+$ states used by Sando *et al.*[2] and in the present study. They differ only in minor details from those arising in the nonradiative scattering calculations. Because of the polarization of H by the He^+ ion, the potential curve for the $A\,^1\Sigma^+$ state contains an attractive long-range component which can support weak quasibound vibrational states that give rise to resonance structure in the cross sections. Shown in Fig. 2 are the radial coupling matrix element for process (1) and the dipole matrix element[2] for processes (2) and (3). Both the nonadiabatic radial coupling and the dipole coupling functions have peaks at $R \simeq 2.0a_0$ and decrease rather rapidly beyond $R \simeq 8a_0$.

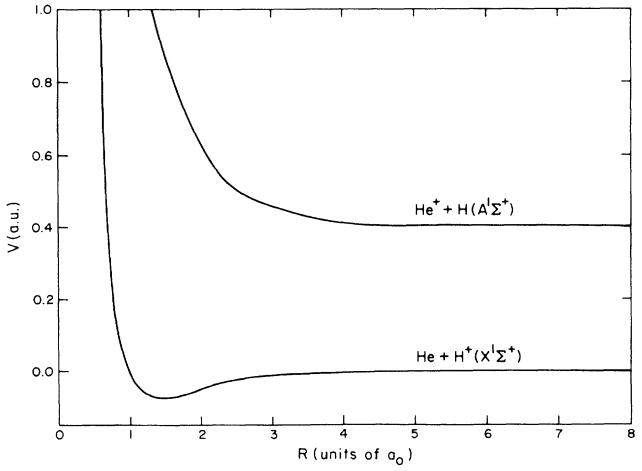

FIG. 1. Adiabatic potential curves of the HeH^+ system.

The calculated cross sections for radiative charge transfer (2) and total radiative decay are illustrated in Fig. 3. The presence of the quasibound rovibrational states in the attractive portion of the $A\,^1\Sigma^+$ potential gives rise to the conspicuous low-energy resonance structures seen in Fig. 3. In Fig. 3 the resonances are seen to occur at collision energies 0.075, 0.23, 1.72, and 5.8 meV. The quantum numbers (v,J) associated with the corresponding quasibound levels in the $A\,^1\Sigma^+$ state are labeled in Fig. 3, where v and J are the vibrational quantum number and rotational quantum number, respectively. Smaller, less conspicuous resonance structures appear at other energies. These resonances contribute to a significant enhancement in the rate coefficients at low temperatures. The cross section for the association process (3) is about twice as large as that for radiative charge transfer at collision energies below 10 meV. Above 10 meV, the radiative charge transfer process dominates and the contribution from radiative association is negligible when the collision energy exceeds 1 eV. Apart from

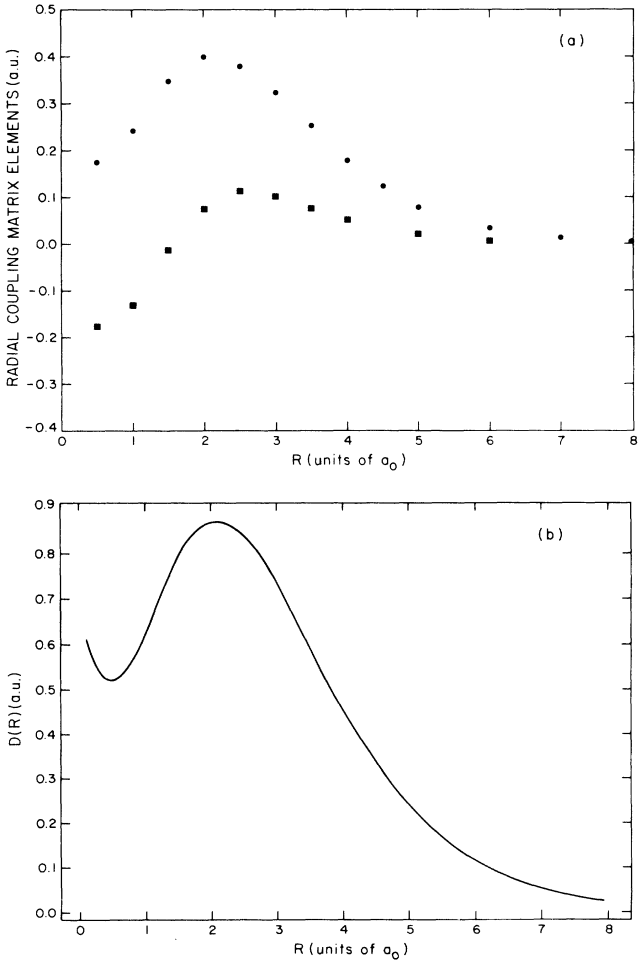

FIG. 2. (a) Nonadiabatic radial coupling matrix elements $\langle X\,^1\Sigma^+|-(\underline{\mathbf{P}}+\underline{\mathbf{A}})|A\,^1\Sigma^+\rangle$ (solid circles) and $\langle A\,^1\Sigma^+|\underline{\mathbf{P}}+\underline{\mathbf{A}}|X\,^1\Sigma^+\rangle$ (solid squares), and (b) the radial transition dipole matrix element.

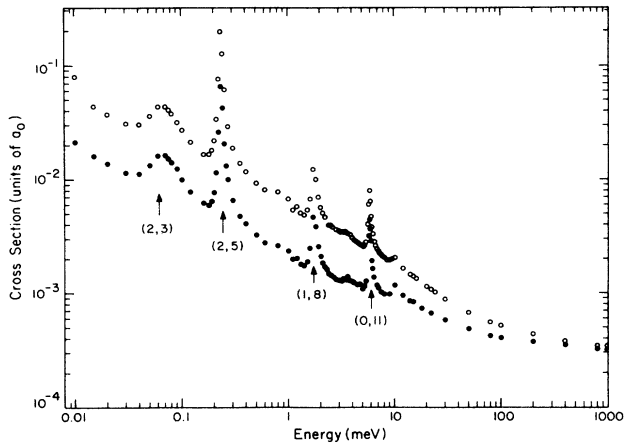

FIG. 3. Radiative charge transfer and total radiative decay cross sections: the solid circles are the radiative charge transfer cross sections, and the open circles are the total radiative decay cross sections. Resonances are labeled by (v,J) where v and J are the vibrational and rotational quantum numbers, respectively.

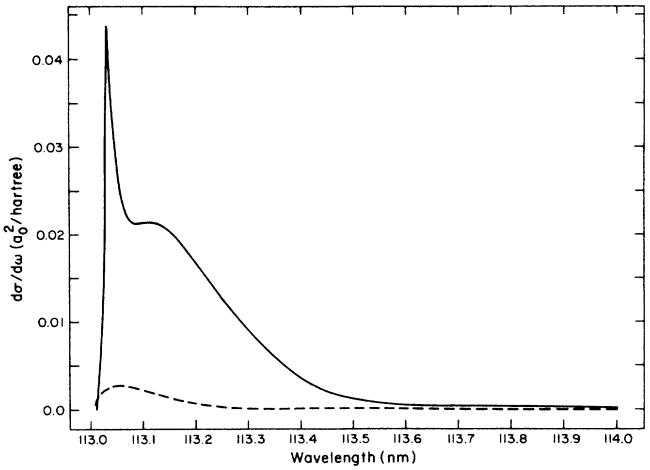

FIG. 4. Spectra for emitted photons in the radiative charge transfer process (2). Comparison between the resonant $v=2$, $J=5$ partial-wave spectra (solid line) to the nonresonant contributions (dashed line), at a collision energy of 0.23 meV.

these resonance structures, the cross sections decrease monotonically as the collision energy increases up to an energy of 1 eV, followed by a slight increase at higher energies. In the region between 2 and 50 eV the radiative charge transfer cross sections have an almost constant value of about 10^{-20} cm^2; at energies greater than 100 eV the cross section decreases as the inverse power of the collision velocity.

The calculated rate coefficients for process (2) and for the total radiative decay rate are listed in Table I. They replace the earlier studies.[2]

In Fig. 4 we present the spectrum for a collision energy of 0.23 meV, which is nearly coincident with the energy of the $v=2$, $J=5$ quasibound resonance level. The resonance spectrum and the spectrum arising from the nonresonant partial waves ($J\neq 5$) are shown separately. The total spectrum (not shown) is dominated by the resonance contribution centered around 113.03 nm, and the peak at 113.12 nm which corresponds to a nearly vertical transition is at the equilibrium separation of the quasibound level. Similar emission spectra are associated with the other peaks in Fig. 3.

TABLE I. Rate coefficients for direct radiative charge transfer and for total radiative decay in units of 10^{-15} cm^3 sec^{-1}.

T (K)	Direct	Total
1	5.36	15.4
10	4.21	11.7
100	4.41	8.34
200	4.50	7.49
400	4.83	7.16
1000	5.99	7.71

For a given partial wave with angular momentum J, the emission intensity is proportional to $|M_{J,J'}(k_a,k_b)|^2$ defined in Eq. (12). The largest contribution to $M_{J,J'}$ comes from the region near the classical turning point of the incoming partial wave in the initial $A\,^1\Sigma^+$ state. Thus $M_{J,J'}(k_a,k_b)$ maps the phase of the outgoing partial wave at the classical turning point of the incoming wave. As we adjust the value of the wave number k_b, $M_{J,J'}(k_a,k_{b)}$ oscillates between a relative maximum and minimum value. Because the frequency of the emitted photon is related to the outgoing wave number k_b by energy conservation

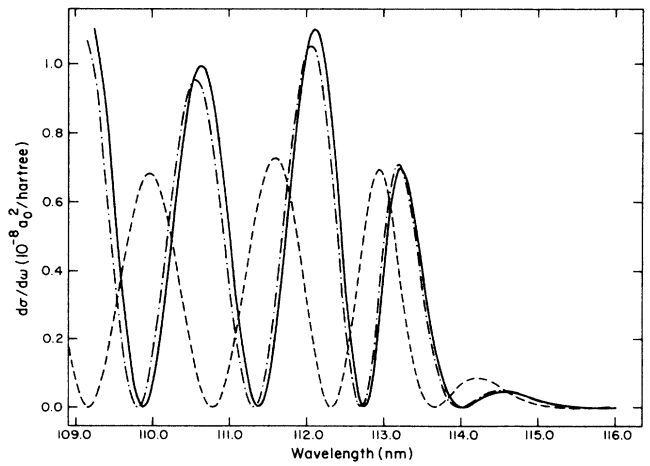

FIG. 5. Spectra for the $J=0$ incoming partial wave at collision energies of 400 meV (solid line), 410 meV (dot-dashed line), and 500 meV (dashed line).

$$\hbar\omega = \hbar k_a^2/2\mu - \hbar k_b^2/2\mu + V_a(\infty) - V_b(\infty)$$

the emission spectrum for a given partial wave exhibits oscillatory structure. It is illustrated in Fig. 5, which shows the emission spectra arising from the $J=0$ partial wave at collision energies of 0.40, 0.41, and 0.50 eV.

To obtain the total emission spectrum, contributions from each partial wave must be summed explicitly as in Eq. (12). Figure 6 shows the total spectrum for a collision energy of 0.4 eV. The spectrum is smooth, except for distinct peaks at discrete wavelengths, with a main peak near 112.95 nm followed by a rapid fall-off at longer wavelengths. The main peak occurs when the transitions occur in the region where the potential curves of the $A\,^1\Sigma^+$ and $X\,^1\Sigma^+$ states are nearly parallel. We propose that the lesser, but prominent, peaks in the short-wavelength region are due to orbiting effects in the outgoing channel. Because the $X\,^1\Sigma^+$ potential curve is attractive for $R > 1.5a_0$, the effective potential $V_{\rm eff} \equiv V_b(R) + J(J+1)/2\mu R^2$ for the Jth outgoing partial wave possesses maxima near the shoulder of the $X\,^1\Sigma^+$ potential curve. If the kinetic energy of a given outgoing partial wave has a value near the potential maximum, then the wave function has a resonancelike structure reflecting the occurrence of orbiting[11] and its amplitude is enhanced. At specific kinetic energies in the exit channel, the overlap integral $M_{J,J'}(k_a,k_b)$ is strongly enhanced when the phase of the outgoing wave is such that it interferes constructively with the incoming wave. This condition will only be satisfied for a limited set of partial waves. When it is met, a peak appears in the photon emission spectrum at the wavelength associated with the corresponding kinetic energy of the exit channel. We have analyzed the emission spectra for individual partial waves and confirmed that the emission peaks occur at frequencies where the outgoing collision energy $\hbar k_b^2/2\mu$ satisfies the conditions required for orbiting. Figure 7 shows the spectra for a collision energy of 1 eV. Because of the averaging effect of the larger number of contributing J values, these peaks are suppressed at higher collision energies, though still present at short wavelengths.

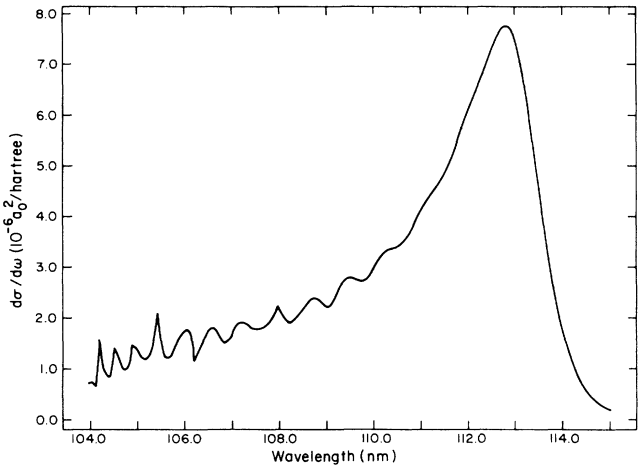

FIG. 7. Emission spectra at a collision energy of 1 eV.

B. Direct charge transfer

The calculated results for the nonradiative charge transfer and the radiative charge transfer cross sections are plotted in Fig. 8 for the energy range from 1 to 100 eV. The nonradiative charge transfer cross sections show a sharp increase above 4 eV as the collision energy increases. In the energy range 5–8 eV, the magnitude of the nonradiative and radiative charge transfer cross sections is comparable with a value of 10^{-20} cm^2. In this

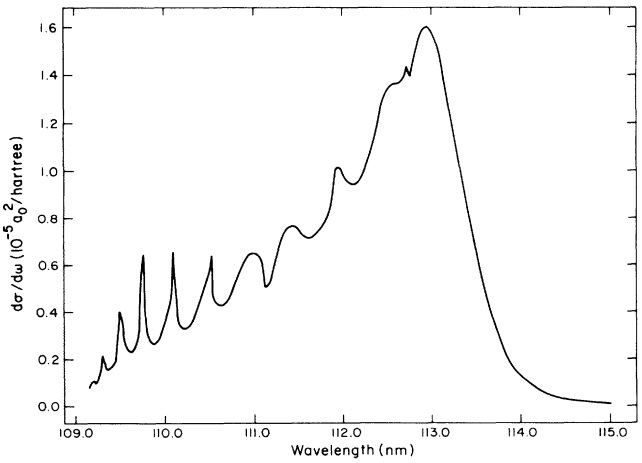

FIG. 6. Emission spectra at a collision energy of 400 meV.

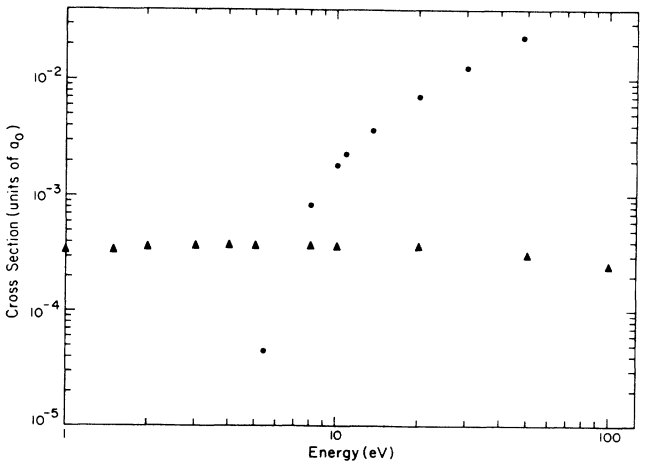

FIG. 8. Comparison between nonradiative (direct) charge transfer cross sections (circles) and radiative charge transfer cross sections (triangles).

overlap region there may occur interference effects between the competing processes and these are not contained in the present theory. Above 8 eV the radiative processes are slow and nonradiative direct charge transfer is the dominant charge transfer process.

We have ignored charge transfer in the triplet scattering channels of the nonadiabatic transition (1). They may become important at collision energies in the keV range.

ACKNOWLEDGMENTS

The work is supported in part by the U. S. Department of Energy, Office of Health and Environmental Research, under Contract No. W-31 10-Eng-38 (M.K.), the Office of Basic Energy Sciences, Division of Chemical Sciences (B.Z. A.D., and N.F.L.), and by the Robert A. Welch Foundation (N.F.L.).

[1]W. Roberge and A. Dalgarno, Astrophys. J. **255**, 489 (1982).

[2]K. M. Sando, R. Cohen, and A. Dalgarno, *Abstracts of Papers, Proceedings of the Sixth International Conference on the Physics of Electronic and Atomic Collisions, Cambridge, MA, 1969,* edited by I. Amdur (MIT, Cambridge, MA, 1969), p. 973.

[3]B. Zygelman and A. Dalgarno, Phys. Rev. A **38**, 1877 (1988).

[4]T. G. Heil, S. E. Butler, and A. Dalgarno, Phys. Rev. A **23**, 1100 (1981).

[5]J. Tan, C. D. Lin, and M. Kimura, J. Phys. B **20**, L91 (1987).

[6]J. B. Delos, Rev. Mod. Phys. **53**, 287 (1981).

[7]W. R. Thorson and J. B. Delos, Phys. Rev. A **18**, 117 (1978).

[8]B. R. Johnson, J. Comput. Phys. **13**, 445 (1973).

[9]B. W. West, N. F. Lane, and J. S. Cohen, Phys. Rev. A **26**, 3164 (1982).

[10]J. S. Cohen and J. N. Bardsley, Phys. Rev. A **18**, 1004 (1978).

[11]N. F. Mott and H. S. W. Massey, *The Theory of Atomic Collisions,* 3rd. ed. (Oxford University Press, Oxford, England, 1965), p. 106.